Talanta 272 (2024) 125772

Contents lists available at ScienceDirect

Talanta

journal homepage: www.elsevier.com/locate/talanta

Gold nanowires-based sensor for quantification of H_2O_2 released by human airway epithelial cells

Bernardo Patella [a,1], Serena Di Vincenzo [b,1], Nadia Moukri [a], Francesco Bonafede [a], Maria Ferraro [b], Valentina Lazzara [c], Maria Rita Giuffrè [d], Sonia Carbone [a], Giuseppe Aiello [a], Michele Russo [e], Chiara Cipollina [b,d], Rosalinda Inguanta [a,b,*], Elisabetta Pace [b]

[a] Department of Engineering, University of Palermo, Palermo, 90128, Italy
[b] Institute of Translational Pharmacology (IFT), National Research Council of Italy (CNR), Palermo, 90146, Italy
[c] Department of Health Promotion Sciences, Maternal and Infant Care, Internal Medicine and Medical Specialties (PROMISE), University of Palermo, Palermo, 90127, Italy
[d] Ri.MED Foundation, Palermo, 90146, Italy
[e] Dipietro Group, Melilli, 96010, Italy

ARTICLE INFO

Keywords:
Gold nanowires
Electrochemical sensors
Hydrogen peroxide
Oxidative stress
Epithelial cells
A549 cells

ABSTRACT

Hydrogen peroxide (H_2O_2) is a biomarker relevant for oxidative stress monitoring. Most chronic airway diseases are characterized by increased oxidative stress. To date, the main methods for the detection of this analyte are expensive and time-consuming laboratory techniques such as fluorometric and colorimetric assays. There is a growing interest in the development of electrochemical sensors for H_2O_2 detection due to their low cost, ease of use, sensitivity and rapid response. In this work, an electrochemical sensor based on gold nanowire arrays has been developed. Thanks to the catalytic activity of gold against hydrogen peroxide reduction and the high surface area of nanowires, this sensor allows the quantification of this analyte in a fast, efficient and selective way. The sensor was obtained by template electrodeposition and consists of gold nanowires about 5 μm high and with an average diameter of about 200 nm. The high active surface area of this electrode, about 7 times larger than a planar gold electrode, ensured a high sensitivity of the sensor (0.98 μA $\mu M^{-1} cm^{-2}$). The sensor allows the quantification of hydrogen peroxide in the range from 10 μM to 10 mM with a limit of detection of 3.2 μM. The sensor has excellent properties in terms of reproducibility, repeatability and selectivity. The sensor was validated by quantifying the hydrogen peroxide released by human airways A549 cells exposed or not to the pro-oxidant compound rotenone. The obtained results were validated by comparing them with those obtained by flow cytometry after staining the cells with the fluorescent superoxide-sensitive Mitosox Red probe giving a very good concordance.

1. Introduction

In the last years, electrochemical sensors have attracted growing attention due to their simplicity, low cost, excellent performances (in terms of sensitivity, selectivity, limit of detection (LOD) and rapidity of response), the possibility of real-time and in situ analysis using small and portable systems [1,2], and the low volume of analysis which makes them particularly useful for applications where the sample availability is a limiting factor [3]. Due to the very high performance, particularly attractive are the electrochemical sensors based on nanostructured materials which have been proposed for the detection of different analytes such as heavy metals, dopamine, hydrogen peroxide, uric acid, ascorbic acid, and so on [4–6]. Different types of active materials have been proposed for sensor fabrication [7,8]. Among them, gold is one of the most used due to its biocompatibility, high electrical conductivity, chemical and electrochemical stability [9]. Furthermore, the gold surface can be easily modified making it very attractive also for immunosensor applications [10,11]. For electrochemical sensors, gold nanoparticles, ranging from 1 to 100 nm, are widely used and different fabrication methods can be found in the literature for their synthesis

* Corresponding author.
E-mail address: rosalinda.inguanta@unipa.it (R. Inguanta).
[1] These authors contributed equally to this work.

https://doi.org/10.1016/j.talanta.2024.125772
Received 30 June 2023; Received in revised form 8 January 2024; Accepted 7 February 2024
Available online 16 February 2024

[12–14]. Instead, even if much investigated, the synthesis of vertically standing gold nanowires and nanotubes (AuNWs, AuNTs) has not been yet optimized [15,16]. This is related to the tendency of gold to deposit in the dendritic form which makes the nanostructures very brittle and unstable [17–19]. Template-assisted electrochemical methods are very efficient in fabricating vertically standing AuNWs and AuNTs [20,21]. Different authors synthesize AuNWs inside the pores of the template (anodic alumina or polycarbonate membrane (PC)) and then dissolve the membrane obtaining a suspension containing AuNWs/NTs to drop-cast on different substrates [15,22]. However, very few works have shown the deposition of vertically standing AuNWs and AuNTs [23,24]. Mollamahale et al. have used a PC template and a gold cyanide solution to deposit self-standing AuNWs attached to a copper current collector [25]. They have obtained well-defined AuNWs but after the complete dissolution of the template, many nanowires broke down resulting in a decrease in electrode performance. To overcome this problem, they suggested to control the etching process, avoiding the total template dissolution. In another study, the same authors [26] have obtained stable nanostructures controlling the rate of the deposition process. Sharma et al. deposited AuNWs into the PC membrane using a mercury drop as a current collector obtaining highly stable NWs [27].

In this work, we have fabricated mechanically stable AuNW arrays to be used as electrochemical sensors for H_2O_2 quantification in cell culture media. Hydrogen peroxide and other reactive oxygen species (ROS) (including superoxide anions ($O_2^{\cdot-}$), hydroxyl radicals ($OH^{\cdot}$)) are generated by the transformation of oxygen through enzymatic and non-enzymatic reactions [28,29]. Many environmental insults (cigarette smoke, infections, pollutants) cause oxidative stress not only by inducing ROS production but also by suppressing the antioxidant response [30]. The imbalance between oxidant and antioxidant systems is a crucial event that compromises airway homeostasis and leads to the activation of innate and adaptive immunity. Therefore, oxidative stress and airway inflammation generate a vicious cycle responsible for disease progression of most chronic airway diseases, such as asthma and Chronic Obstructive Pulmonary Disease (COPD) [31]. In this respect, the assessment of airways oxidative homeostasis may provide an efficient tool for monitoring disease onset, progression and response to therapy. Therefore, the development of novel diagnostic tools for detecting in an easy way oxidative stress within the airways is of great interest. Hydrogen peroxide is an interesting biomarker for oxidative stress monitoring because it is among the less unstable ROS and diffuses through the cellular membrane, allowing its measurement in the extracellular space. Different types of electrochemical sensors were developed to quantify H_2O_2 [32,33]. Herein the attention has been focused on the development of vertically standing AuNWs arrays to obtain a sensor with high sensitivity attributable to the electrocatalytic properties of nanostructured gold towards the reduction of H_2O_2 [34–36] and to the high surface area typical of nanostructured electrodes [37].

A systematic investigation was conducted on the electrodeposition of AuNWs into PC membrane. In particular, the effect of deposition time, deposition potential, gold precursor concentration and solution pH was evaluated. The optimized nanostructured electrode was used to quantify H_2O_2 in aqueous solutions, using the chronoamperometry technique, to obtain the main features of the sensor such as sensitivity, LOD, linear range and selectivity. To demonstrate the applicability of the sensor in real operating conditions, H_2O_2 released by the human airway cell line A549 treated or not with the pro-oxidant rotenone, was quantified. The results obtained with the AuNWs-based sensor were compared with those obtained by flow cytometry which represent the current standard for intracellular ROS quantification.

2. Experimental

2.1. AuNWs synthesis and characterization

Commercial polycarbonate membranes (Poretics®) with a nominal mean pore diameter of about 200 nm and a thickness of 6 μm, were used as templates for the electrodeposition of AuNWs. One membrane surface was sputtered (for 3 min) with a thin layer of gold to make it conductive. On this surface, a copper current collector was deposited by galvanostatic deposition at −8 mA/cm^2 for 1 h in a solution of 0.2 M $CuSO_4{\cdot}5H_2O$ + 0.1 M H_3BO_3. The deposition was performed using a Pt mesh, as the counter electrode, and a PAR potentiostat/galvanostat (PARSTAT, mod. 2273). On the other template surface, the electrodeposition of gold nanostructures was performed using a Pt mesh as a counter electrode and an Ag/AgCl reference electrode. The electrodeposition of gold nanostructures was performed by potentiostatic mode in a deposition area of about 10 cm^2. The effect of the gold precursor concentration (from 0.1 to 10 mM), the deposition solution (using HCl 0.1 M (pH 1) or acetate buffer solution (ABS, pH 5.4)), the deposition time (from 30 to 90 min) and the applied potential (from −150 to −450 V vs Ag/AgCl) was evaluated. After Au deposition, the template was etched in pure tetrachloromethane. In Fig. S1 the scheme of template electrosynthesis was reported. The electrodeposition of both the current collector and AuNWs was performed at room temperature.

Morphology was analyzed through scanning electron microscopy (SEM), using a FEI FEG-ESEM (mod. QUANTA 200) equipped with a detector for Energy Dispersive Spectroscopy (EDS). X-ray diffraction (XRD) was carried out using a RIGAKU diffractometer (model: D-MAX 25600 HK). All the diffraction patterns were obtained in the 2θ range from 10° to 90° with a step of 0.004° and a measuring time of 0.067 s for each step, using the copper Kα radiation (λ = 1.54 Å). Diffraction patterns were analyzed by comparison with the ICDD database [38].

2.2. Sensor fabrication and characterization

After template dissolution, AuNWs were cut with a circular shape (diameter 1.2 cm) using a CO_2 laser cutter, assembled with copper tape into glass support and insulated with a lacquer (the exposed working area is 0.785 cm^2). All the potentials are referred to the saturated calomel electrode (SCE). To estimate the electrochemical active surface area of the electrode, cyclic voltammetry (CV) was carried out in phosphate buffer solution (PBS) in the potential range from 0 to 0.5 V vs SCE at different scan rates (from 1 to 1000 mV s^{-1}) where no faradaic reactions occur. For comparison, the same experiment was carried out using a planar gold sheet. CVs at different scan rates in PBS pH 7.4 with 1 mM H_2O_2 were also carried out in the potential range from −0.8 to +0.8 V vs. SCE.

Hydrogen peroxide was quantified using chronoamperometry (CH) as the electrochemical technique. The repeatability of the electrode was verified by calibrating the same electrode several times. The reproducibility was proved by calibrating different sensors prepared in the same way. The LOD was calculated by measuring the standard deviation of the blank using the following equation:

$$LOD = 3.3 * SD / S$$

where SD is the standard deviation of the blank and S is the slope of the calibration line. The electrode selectivity to different chemicals (lactic acid, uric acid, ascorbic acid, 4-(2-hydroxyethyl)-1-piperazine-ethanesulfonic acid (HEPES), sodium chloride, sodium nitrate and glucose, all from Alfa Aesar) was studied. These chemicals were analyzed at a concentration 10 times higher than the H_2O_2 to simulate the worst conditions. The interference to Rotenone (R8875, Sigma-Aldrich) was also verified.

The AuNWs-based sensor was used to quantify H_2O_2 released by A549 cells. For these tests, the electrode was immersed in the PBS and

the CH was carried out until the stabilization of the current density. Then, the conditioned medium (0.5 mL) collected during cellular growth was spiked into the blank solution (PBS) to quantify the H_2O_2 released from the cells during their growth.

To validate the measurements made by the sensor, solutions containing different concentrations of H_2O_2 in RPMI medium were analyzed in parallel with both the sensor and the biochemical assay based on the Amplex Red reagent (Amplex™ Red Hydrogen Peroxide/Peroxidase Assay Kit-Invitrogen). The assay was performed following the manufacturer's instructions.

All electrochemical tests were done in the air and were performed in a stirred solution (at 600 rpm) which guaranteed the continuous recirculation of the electrolyte. The stirred solution was used because it allowed to obtain greater sensitivity of the sensor. In particular, we found that the electrode sensitivity increased by a factor of 2.13 in comparison to the unstirred solution due to the better transport of H_2O_2 to the sensor surface.

2.3. Cell culture, cell stimulation and measure of mitochondrial ROS

The lung adenocarcinoma cell line, A549 (American Type Culture Collection (ATCC)), was used in this study. A549 cells were maintained in a humidified atmosphere of 5% CO_2 in air at 37 °C and were cultured as adherent monolayers. RPMI medium supplemented with 10% heat-inactivated (56 °C, 30 min) fetal bovine serum (FBS), penicillin–streptomycin, 1% MEM (non-essential amino-acids) and 2 mM L-glutamine (all from Euroclone) was used for culturing cells.

A549 cells were cultured to confluence, then the serum was reduced from 10% to 1% and the cells were stimulated or not with 2.5 μM of Rotenone for 2 h. At the end of stimulation, the conditioned medium was collected for H_2O_2 quantification using the sensor and the cells were collected to measure intracellular mitochondrial superoxide by flow cytometry. In brief, cells were harvested by trypsinization and incubated with a solution containing 3 μM of Mito-SOX™ Red probe which detects mitochondrial superoxide (15 min, at 37 °C). Then cells were washed, and the fluorescence was measured using the flow cytometer CytoFLEX (Beckman Coulter). The results were expressed as the mean of fluorescence intensity (MFI).

A549 cells were also used to assess the impact of the sensor when operating directly in the cell culture growth medium on cell viability. To this purpose, the sensor was submerged directly in the culture medium of a 6-well plate with A549 cells, paying attention not to disturb the cell monolayer. Cell viability was evaluated by measuring the release of Lactate dehydrogenase (LDH) assay (CytoTox 96® Non-Radioactive Cytotoxicity Assay – Promega) in cell culture medium (N = 3) at the time of the introduction of the electrode (T 0 h) and after 24 h (T 24 h). The assay was performed following the manufacturer's instructions.

3. Results and discussion

3.1. AuNWs synthesis and characterization

To optimize the fabrication of AuNWs, different parameters of the electrodeposition process were studied. The first investigated parameter was the effect of the concentration of the gold precursor used to prepare the deposition solution. Tests were carried out applying a constant potential of −150 mV vs Ag/AgCl, dissolving different amounts of $HAuCl_4$ into ABS for 30 min. In Fig. 1 (Fig. S2) the SEM images of the samples obtained at different concentrations of gold precursor were reported.

A very low concentration of gold precursor (0.1 mM) led to very short nanostructures (Fig. S1A) and thus a very low surface area [39]. The highest tested gold concentration (10 mM) led to a too-fast deposition that reached the top of the membrane with consequent deposition of gold on its top, Fig. 1A. In this case, the deposit has the typical fern-leaf morphology [40]. This morphology is formed because the kinetically slow stage is that of dendritic growth, while nucleation is the fast stage [41]. At intermediate concentrations, different results were obtained. At 0.5 mM AuNTs were formed, (Fig. S2B). However, the wall thickness of the nanotubes was too small, and this is probably the cause of their collapse after the dissolution of the template. The deposition carried out with 1 mM of $HAuCl_4$, Fig. 1B, led to well-defined AuNTs with a uniform length. Thus, the best concentration of Au precursor was 1 mM because ensured the formation of a regular array of Au nanostructures.

However, the electrode reproducibility was not satisfying due to the intrinsic fragility of nanotubes which break very easily with consequent modification of the surface area of the electrode and its performance. For this reason, to obtain stronger nanostructures, the effect of applied potential in the range from −150 mV to −450 mV vs. Ag/AgCl was investigated (Fig. 2A and Fig. S3). The applied potential had little influence on the nanostructure morphology. All the investigated potentials resulted in the formation of the nanotube (NT) shape. In particular, from −150 mV to −300 mV vs Ag/AgCl, NTs very similar to those of Fig. 1B were obtained. Some differences were observed at −300 mV, which resulted in an array with slightly longer and thicker-walled NTs compared to the nanostructures obtained at −150 mV, and some

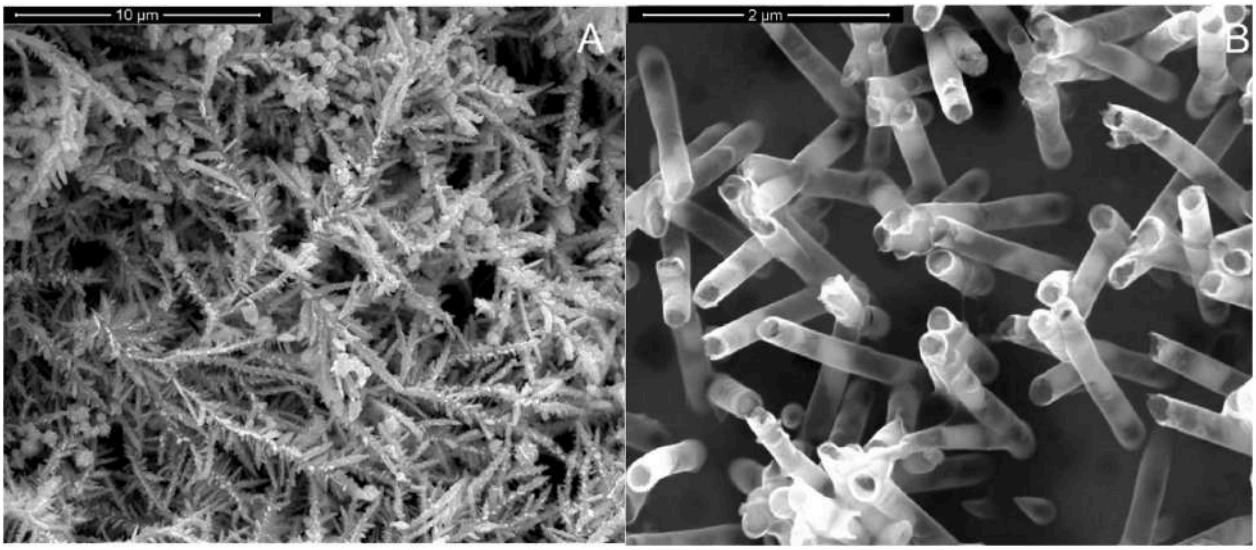

Fig. 1. Morphology of Au nanostructures obtained at −150 mV vs Ag/AgCl for 30 min with different concentrations of $HAuCl_4$: A) 10 mM and B) 1 mM.

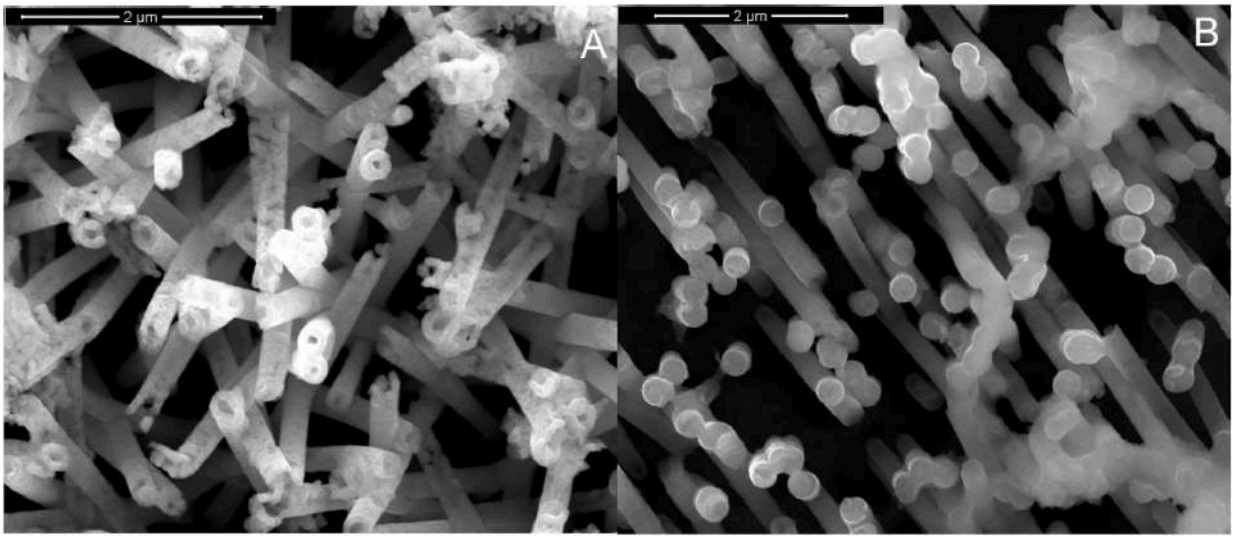

Fig. 2. Morphology of Au nanostructures obtained at −300 mV vs Ag/AgCl for 30 min in different deposition baths: A) 1 mM $HAuCl_4$ and B) 1 mM $HAuCl_4$ + 0.1 M HCl +0.1 M KCl (pH 1).

irregular nanotube walls at the end. At more cathodic potentials, NTs with a very thin wall were obtained. Those NTs were too fragile, and they were destroyed during the etching of the PC template and the subsequent washings in the organic solvent. The formation of very thin NTs is due to the concomitant evolution reaction of hydrogen whose driving force increases as the applied potential increases [42]. The hydrogen bubbles tend to accumulate inside the pores of the membrane, limiting the deposition of gold in the gap between the pore wall and the gas bubbles [43]. From these results, a potential of −300 mV was selected for further experiments because it allows the NTs deposition with thicker walls.

To further improve the electrode morphology, the deposition solution was changed using a solution of 1 mM of $HAuCl_4$ + 0.1 M HCl +1 M NaCl (pH 1, Fig. 2B). This acidic solution was selected because it allowed to obtain gold nanowires (NWs) as reported in Ref. [39]. The morphology of the obtained electrode is shown in Fig. 2B. The nanostructures preferentially had a NW shape although with a different height. There were also some NTs with very thick walls.

Finally, the effect of deposition time was studied. The morphology of the nanostructures obtained using different times of deposition remained substantially unchanged (Fig. 3). A slightly different shape (Fig. S4) was observed at the top of the NWs with increasing deposition time. As it is better evident from Fig. 3B, the nanostructures have, in the upper part, an internal profile with a conical shape. This is attributable to a different growth rate along the axis of the channels compared to the growth in the radial direction, again attributable to the obstacle deriving from the hydrogen bubbles. Increasing the deposition time from 30 to 90 min, the average NW length increased from about 1.5 μm to 5 μm. Considering that longer NWs lead to a sensor with a higher surface area, 90 min was selected as the best deposition time.

Considering the above results, the final conditions to obtain vertically standing AuNWs arrays by template deposition are the following:

- Deposition solution: 1 mM $HAuCl_4$, 0.1 M HCl and 1 M NaCl;
- Deposition potential: −300 mV vs Ag/AgCl;
- Deposition time: 90 min.

Fig. 4 shows SEM images of the optimized electrode at different magnifications. The images were obtained with a tilt angle of 30°. Fig. 4A and B shows the top view of the nanostructured electrode while

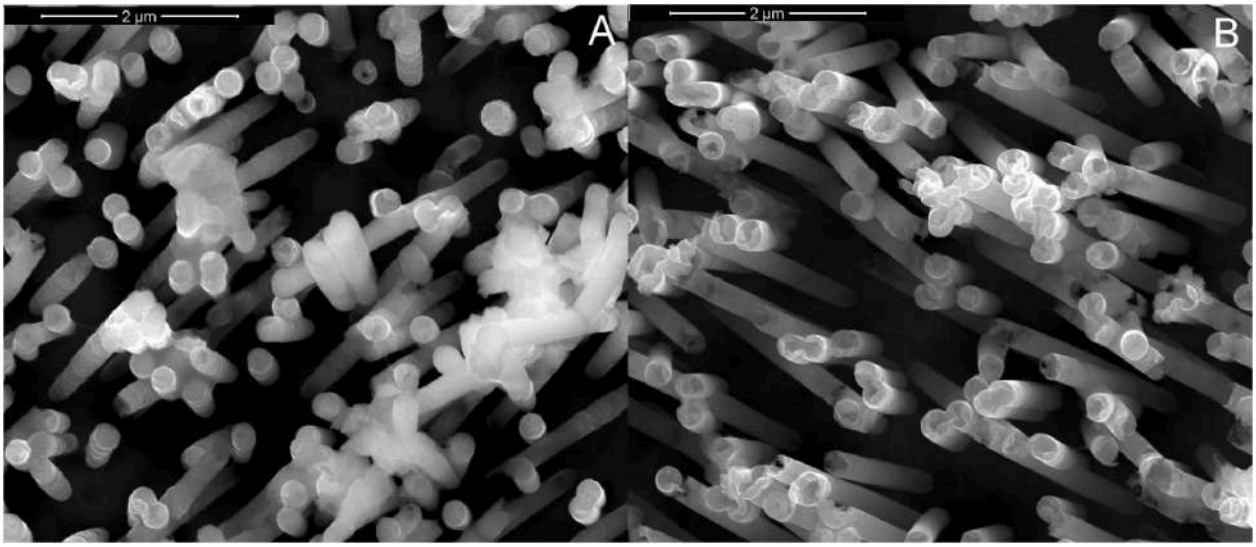

Fig. 3. Morphology of Au nanostructures obtained at −300 mV vs Ag/AgCl at different deposition times: A) 60 min and B) 90 min.

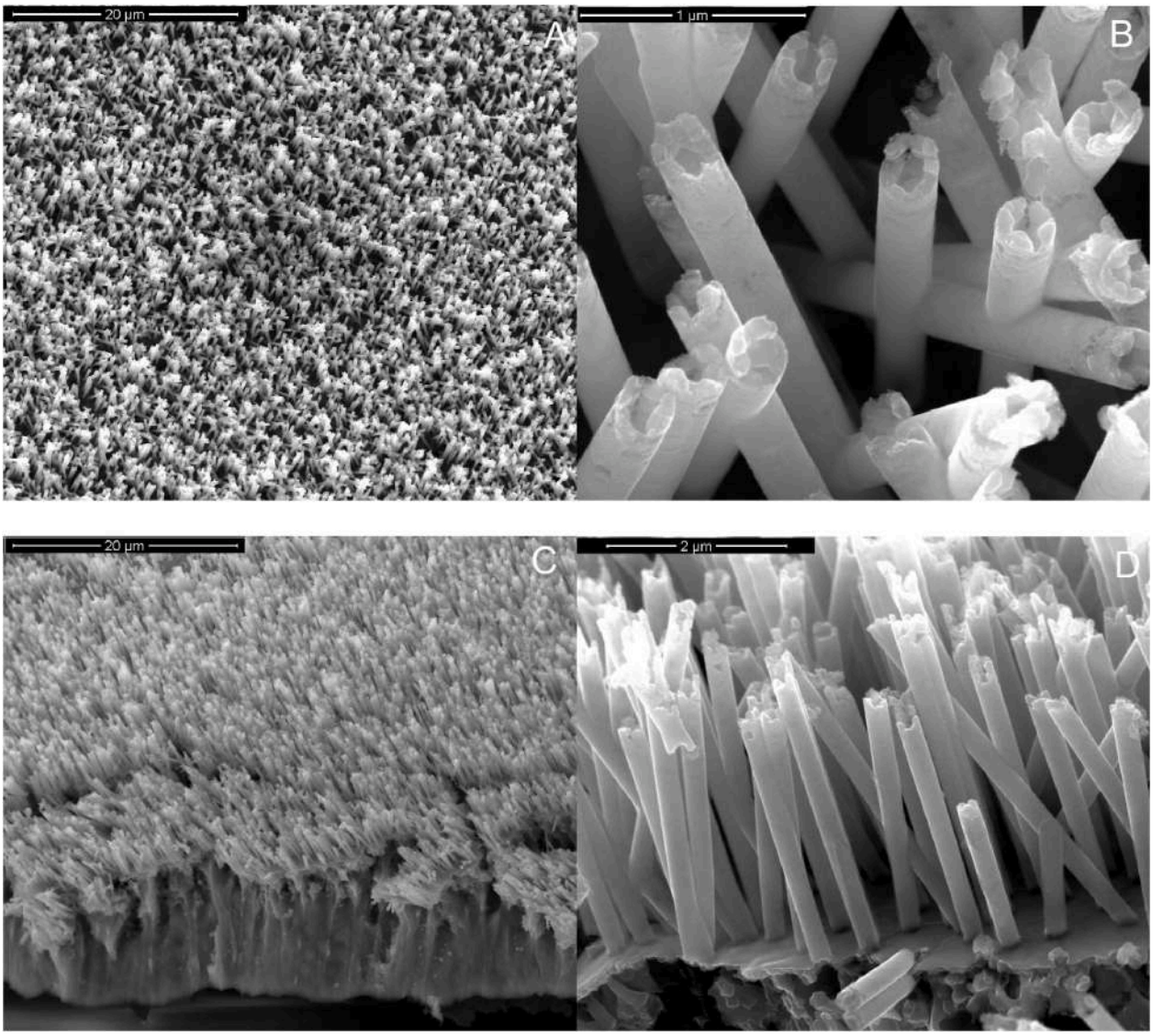

Fig. 4. SEM images of the optimized Au nanowires: A-B) top view, C-D) cross-section view.

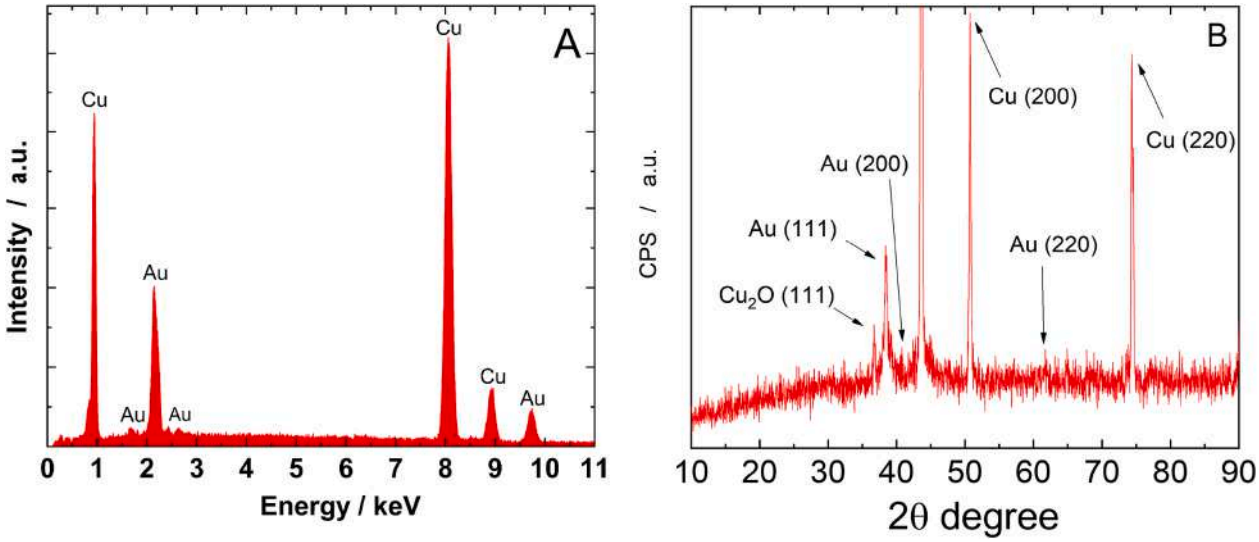

Fig. 5. A) EDS spectrum and B) XRD pattern of the optimized electrode. (The entire XRD pattern of the sample was reported in Fig. S5).

in Fig. 4C and D the cross-sectional view is reported. In Fig. 4A and C, it can be observed that the Cu current collector is uniformly covered by AuNWs. The Cu collector, about 20 μm thick, is continuous, uniform, compact and free of cracks or fractures. Fig. 4B highlights the morphology of the NWs which have an almost regular cylindrical shape except for the final part near the top which has an internal conical shape, as above discussed. Compared to Fig. 3B, the internal conical shape is better visible here due to the longer deposition time. In fact, as the deposition time increases, the accumulation of hydrogen inside the channels of the template increases and consequently the axial growth is more favored than the radial one. In addition, in Fig. 4B, some interconnections between different wires, due to the shape of PC template channels, are also clearly visible. Nanowires have an almost uniform diameter of about 200 nm like the nominal diameter of the template. The high-magnification image of Fig. 4D shows that nanowires are firmly connected to the current collector and have a low surface roughness. In Fig. 4C and D, the presence of some broken nanowires is due to the preparation of the cross-section of the sample for SEM analysis, which was prepared by simply tearing off a flap of the sample.

The optimized AuNWs-based electrode was analyzed using EDS and XRD. By EDS, different areas were analyzed to verify electrode homogeneity. In the EDS spectrum, Fig. 5A, the presence of Cu was due to the copper current collector, while the Au peak was due to AuNWs. No other peaks were highlighted, except traces of C and O (for KeV<0.5) due to polycarbonate residues left on the electrode after the template dissolution. The XRD pattern shows the presence of poly-crystalline copper and gold (Fig. 5B and Fig. S5) [38]. In particular, Cu peak positions coincide with those of metallic copper with cubic structure (XRD card 04–0836). The peak at about 36.7° is relative to the main diffraction peak of Cu_2O (XRD card 05–0667) due to the formation of native oxide of the copper in air [44]. The cubic structure of Au has been identified through the peaks located at 38.48° related to the (111) plane (XRD card 04–784). The second peak at 44.38°, relative to the (200) plane is masked by the main copper peak which is very intense. Through the line broadening at half the main intensity Au peak and using Scherrer's equation, it was possible to calculate the main size of AuNW grains, obtaining a value of about 15.84 ± 0.5 nm.

The electrochemical surface area of the optimized electrode was evaluated by recording CVs at different scan rates (from 10 to 1000 mV s^{-1}) in the potential range from 0 to 0.5 V vs SCE, where no faradaic reactions occur [45]. PBS solution was used as the electrolyte. For comparison, also planar gold was tested. Results are shown in Fig. 6. Fig. 6A and B shows the CV curves at different scan rates for AuNWs and planar gold, respectively. From these CVs, the double-layer capacitance (C_{dl}) was calculated by measuring anodic and cathodic current density differences at 0.25 V vs. SCE and results are shown in Fig. 6C.

For both electrodes, a linear dependence with the scan rate was found. The slope of these lines is related to the C_{dl}. The C_{dl} of planar gold was about 7 times lower compared to AuNWs-based electrodes. This is a good result imputable to the very large surface area of the AuNWs by which the performance of the sensor depends on [46]. The obtained surface increase factor value is plausible because it is in good agreement with the value calculated from the analysis of SEM images using the following equation proposed in [47].

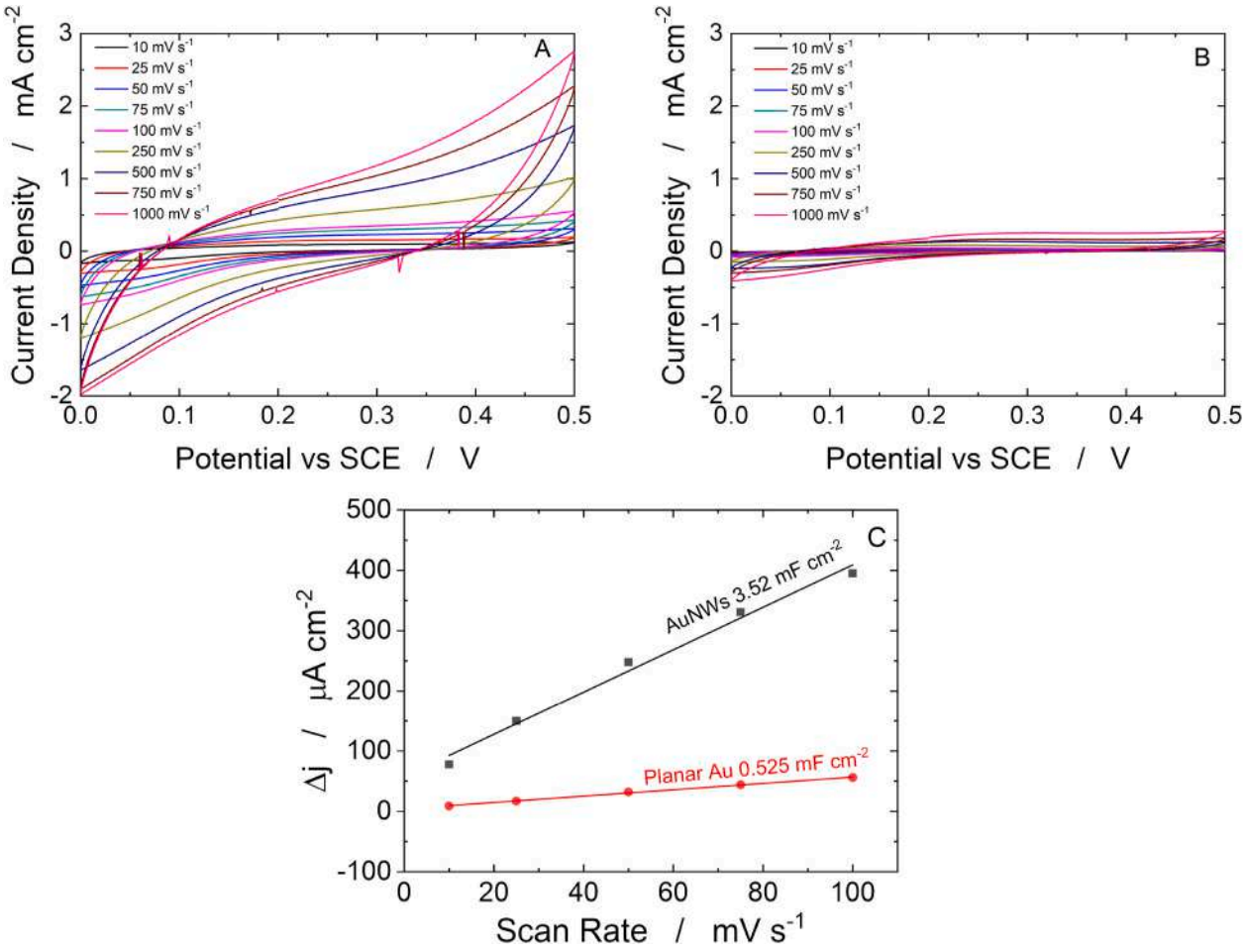

Fig. 6. CVs at different scan rates in PBS solution using A) AuNWs and B) planar gold. C) Specific capacitance of electrodes evaluated by double-layer capacitance at 0.25 V.

$$Surface\ Area = A + \frac{\pi d_{NW_s} h_{NW_s} A}{sen\alpha (x_{NW_s} + d_{NW_s})^2}$$

where A is the geometric area of the electrode, d_{NW_s} and h_{NW_s} are, respectively, the mean diameter and height of the nanowires, x_{NW_s} is the average spacing of the nanowires, α is the tilt angle (30°) of the specimen during the SEM analysis. Using this equation, a total surface area of NWs of 5.18 cm^2, 6.6 times higher than the geometrical one, was calculated.

To study the electrochemical oxidation/reduction of H_2O_2 using herein-developed AuNW-based electrodes, CVs at different scan rates, from 25 to 500 mV s^{-1}, in the potential range from −0.8 to 0.8 V vs SCE were also carried out into a solution of PBS containing 1 mM H_2O_2, Fig. 7. By increasing the scan rate, the peak current density increased. At the same time, the oxidation potential peak shifted towards more anodic value (from about 47 to about 410 mV vs SCE), while the reduction peak moved to more cathodic potentials (from about −395 to about −711 mV vs SCE), [48]. The oxidation and reduction peak current densities were plotted against the square root of the scan rate. A linear relation was found, suggesting that the oxidation and reduction of H_2O_2 is a diffusional controlled process according to the results obtained by Zhang et al. [49] in the case of Au nanocages. The logarithm of the reduction peak potential was plotted against the logarithm of current density and a linear trend was found. The slope of the linear regression corresponds to the heterogeneous charge transfer coefficient (α) [45]. A value of 0.532 was measured which is very close to 0.5. This result is a further confirmation that the electrochemical reduction of H_2O_2 over AuNW-based electrodes is a diffusion-controlled process.

3.2. Hydrogen peroxide quantification

The quantification of H_2O_2 was carried out in a solution stirred at 600 RPM to achieve better analyte transport on the entire active surface area of the sensor. The detection of H_2O_2 was performed by chronoamperometry by applying −0.35 V vs. SCE in PBS. Fig. 8A shows the chronoamperogram at increasing H_2O_2 concentration. After the start of the test, the sensor output stabilized after about 200 s. Starting from this time, H_2O_2 was inserted at regular time intervals of 60 s. After the addition of H_2O_2 into the solution, the current density increased suddenly with a rapid stabilization lasting less than 5 s. This is a very rapid response, faster than previously reported ones [50,51]. The calibration of the AuNW-based sensor was carried out three times with the same electrode to calculate the sensor repeatability, Fig. 8B. All experiments were fitted with an $R^2 > 0.998$. A very wide linear range was found, from 10 μM to 10 mM. The mean sensitivity of the AuNW-based sensor was 0.98 ± 0.1 mA cm^{-2} mM^{-1}. For each calibration experiment a very low standard deviation of about 3% was calculated. A LOD of 3.21 ± 0.2 μM was found. The obtained sensitivity and LOD values were significantly improved compared to those obtained using a sensor based on reduced graphene oxide and gold nanoparticles [52], as well as compared to many other Au-based sensors (see the comparison table, Table S1, reported in the supplementary material).

The electrode repeatability was studied by testing the same electrode 10 times. Between tests, the sensor was simply cleaned using distilled water. From these tests, it was observed that the sensitivity of the sensor did not change (deviation <3%) therefore demonstrating the excellent

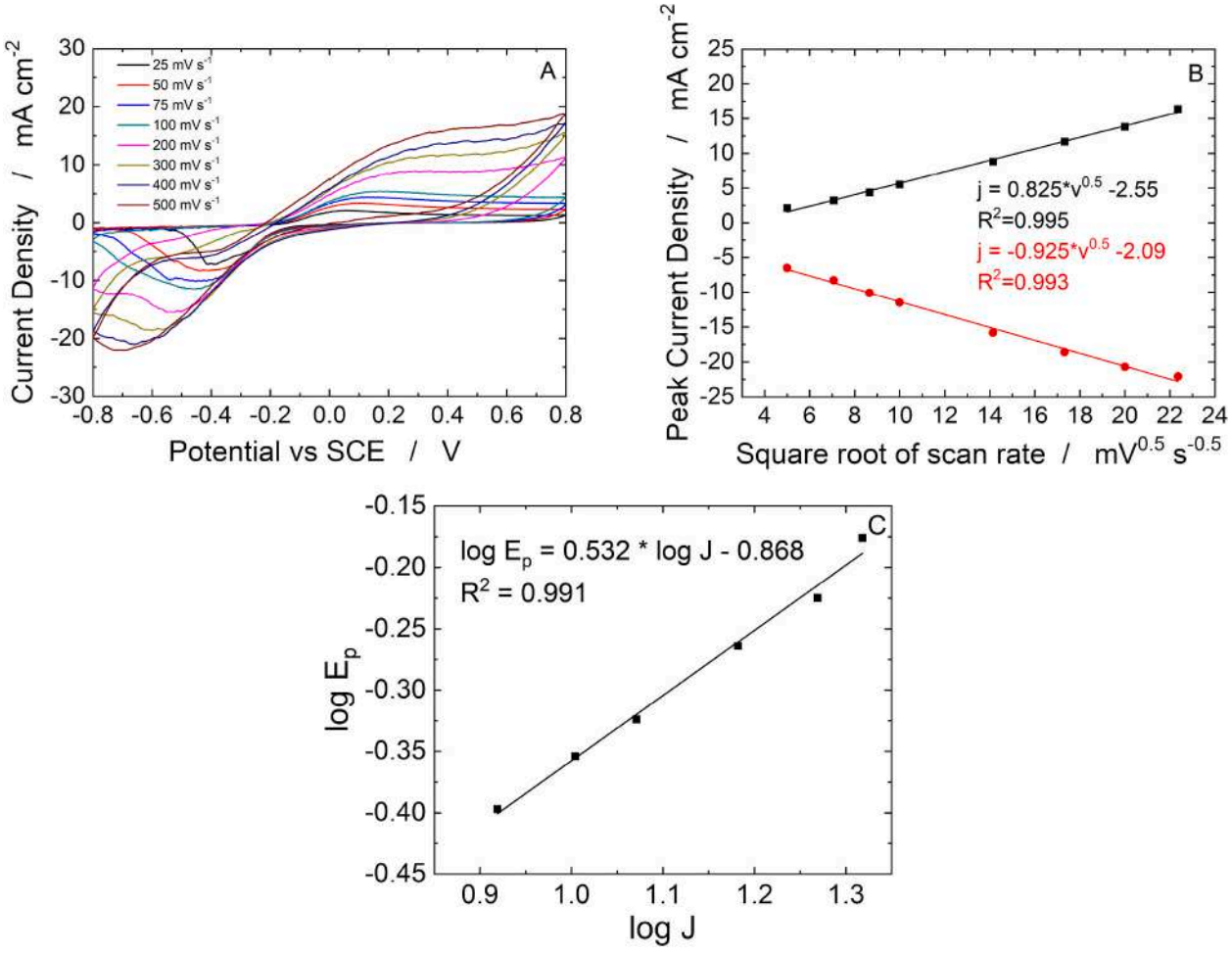

Fig. 7. A) CVs at different scan rates using AuNWs in PBS and 1 mM hydrogen peroxide. B) Peak current densities vs square root of scan rate. C) log E vs log J for reduction of hydrogen peroxide.

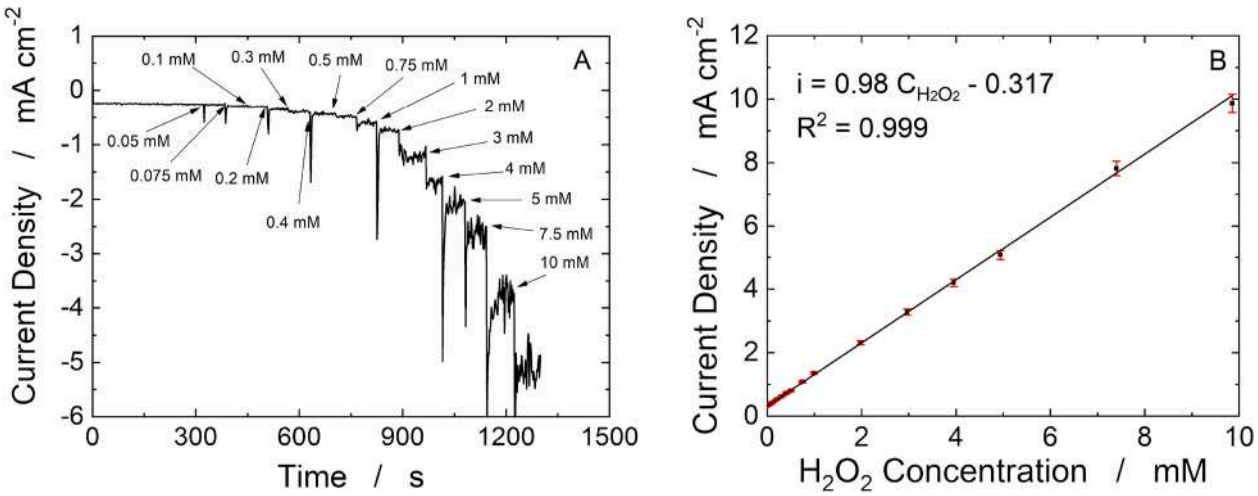

Fig. 8. A) Chronoamperogram at increasing concentrations of hydrogen peroxide. B) Calibration line.

repeatability of the electrode. To study the sensor reproducibility, three different electrodes were fabricated and used to build the calibration line. Results showed a sensor reproducibility of about 7% confirming that the electrode fabrication method was very reproducible. The electrode selectivity was tested towards ascorbic acid, uric acid, lactic acid, HEPES, sodium nitrate and glucose, Fig. 9a. The sensor selectivity was verified for two different concentrations of H_2O_2 (0.1 mM, and 1 mM), and the tests were carried out in PBS. The possible interferents were tested at very high concentrations, 10 times (1 mM and 10 mM) higher than that of H_2O_2, higher than those normally present in the real samples to simulate the worst conditions. Rotenone, used to induce oxidative stress during cellular growth, was also tested as a possible interferent, Fig. 9b. After the initial output sensor stabilization, 0.1 mM H_2O_2 was spiked into the solution and the signal was left to stabilize for 100 s. Then, 1 mM of each chemical was added to the solution every 60 s. The same procedure was followed for the higher concentration. As it can be observed in Fig. 9a, the current density did not change after the addition of the chemicals, while it continued to vary after the addition of H_2O_2 according to the calibration line. This is a very important result because it demonstrates that the electrode possesses high selectivity for H_2O_2 detection. It is essential to highlight that, to add 10 mM of the interfering agent, 1 mL of the respective solution was spiked into the electrochemical cell (initial volume 35 mL). The spiking of this high volume leads to a dilution of H_2O_2 concentration (≈3% for each spike). This explains the slight decrease of current in Fig. 9a. Also in the case of Rotenone, Fig. 9b, no interference was observed.

Table 1 resumes all the features of the proposed sensor for the detection of H_2O_2. The values expressed in % indicate the variation of the current density.

The proposed sensor was used to quantify H_2O_2 released by human airway cellular models. Prior to perform these tests, to confirm the correct operation of the sensor, an identical set of solutions, containing different amounts of H_2O_2 in RPMI (the medium used for the cellular growth), was analyzed both with the sensor and with a selective biochemical assay for H_2O_2, Amplex® Red. From Fig. S6 it can be observed that a good agreement in the results of the two methods was obtained. Consequently, it can be concluded that the sensor was able to quantify H_2O_2 with results comparable to those obtained using a classical and established biochemical assay. We also evaluate the influence of the operation of the sensor on the cell viability, performing the electrochemical test directly on the culture plates. Results showed that the operating sensors had no impact on cell viability (Fig. S7).

The sensor was thus used to quantify H_2O_2 in the medium used for cellular growth. In detail, we used the human lung adenocarcinoma

Table 1
Features of Au NWs for electrochemical quantification of hydrogen peroxide.

Sensitivity mA mM^{-1} cm^{-2}	LOD μM	Repeatability %	Reproducibility %	Selectivity %
0.98 ± 0.1	3.21	<3	7	<1

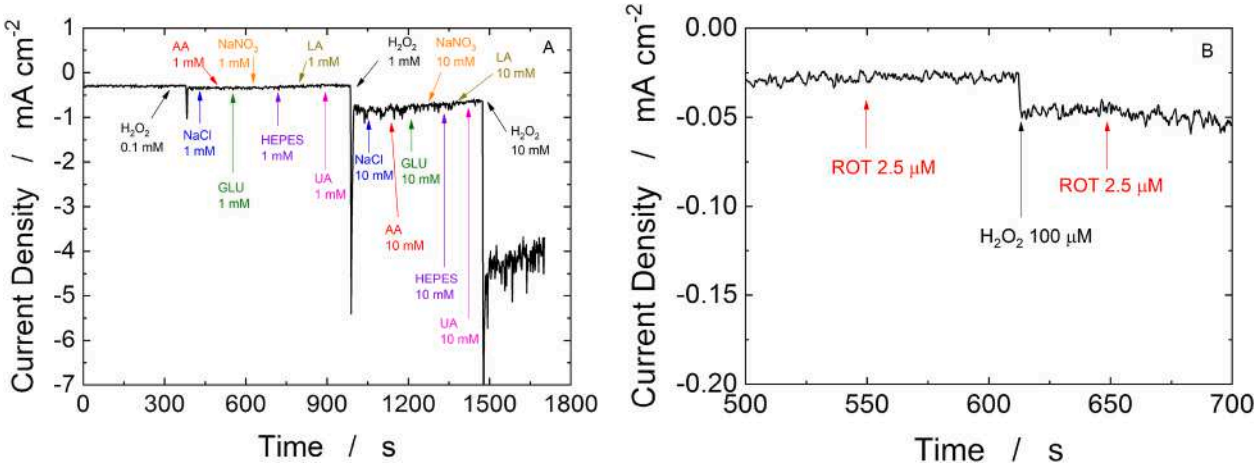

Fig. 9. Selectivity test toward different interfering species (A) and toward Rotenone (B).

A549 cells treated or not with 2.5 μM of Rotenone, a chemical causing mitochondrial damage and consequent high oxidative stress. The medium from treated and not-treated cells was spiked in the cell containing PBS as blank. The dilution factor was 1/70, so the calibration line obtained in PBS was used to quantify the H_2O_2. As it can be observed in Fig. 10A, after the addition of the conditioned medium of non-treated A549 cells, the current density did not change, suggesting that the concentration of H_2O_2 in this sample was lower than the sensor LOD. When the conditioned medium of rotenone-treated A549 cells was added, the current density increased after each addition, with an average value of about 6.4 ± 2.54 μA cm^{-2}. This result indicated that rotenone caused an increase in H_2O_2 release in A549 cells. Using the calibration line, Fig. 8B–a concentration of 6.52 μM was measured. Considering the dilution factor (for each addition 0.5 mL of sample was added to 35 mL of pure medium) the real concentration of H_2O_2 in the conditioned medium of rotenone-treated A549 cells was 457.4 ± 182 μM.

Rotenone induces oxidative stress by blocking the mitochondrial respiratory chain [53,54] leading to an increase of intracellular ROS including H_2O_2 (being H_2O_2 a product of superoxide dismutation) which diffuses through the cell membrane. The results reported in Fig. 10A and B show that the AuNW-based sensor was able to detect the rotenone-induced oxidative stress and this was obtained by performing a simple analysis of the conditioned medium. To validate these results and confirm that the measured extracellular increase of H_2O_2 reflected an increase in intracellular oxidative stress, a flow cytometric analysis was performed. To this purpose, after the collection of the supernatants required for the sensor tests, the cells were harvested and stained with the mitochondrial superoxide-sensitive fluorescent probe Mitosox Red. The results obtained with this approach, which is currently considered the gold standard for intracellular mitochondrial ROS quantification, confirmed that rotenone-induced a significant increase in mitochondrial superoxide generation compared to non-treated cells (Fig. 10C–D).

Overall, these results support that the proposed AuNW-based sensor can be applied for the monitoring of cellular oxidative stress. The use of the sensor provides several advantages compared to currently used flow-cytometric or other biochemical approaches. It is faster because requires only one step (compared to the multiple steps necessary for the flow cytometry approach) and it is a conservative approach because cells remain undisturbed after the removal of the conditioned medium. In addition, the assay is more cost-effective. Therefore, future applications of the sensor may be foreseen for monitoring of oxidative stress.

4. Conclusions

In this work, an AuNW-based electrode was fabricated by template electrosynthesis to use it as a sensor for the detection of hydrogen peroxide released from human lung adenocarcinoma cells (A549). Different parameters of the electrodeposition process (concentration of the gold precursor, applied potential, pH of the solution and deposition time) were optimized to obtain an electrode consisting of mechanically resistant AuNWs attached to the current collector. The optimized electrode was characterized through different techniques that showed the formation of an array of crystalline AuNWs about 5 μm long and with an

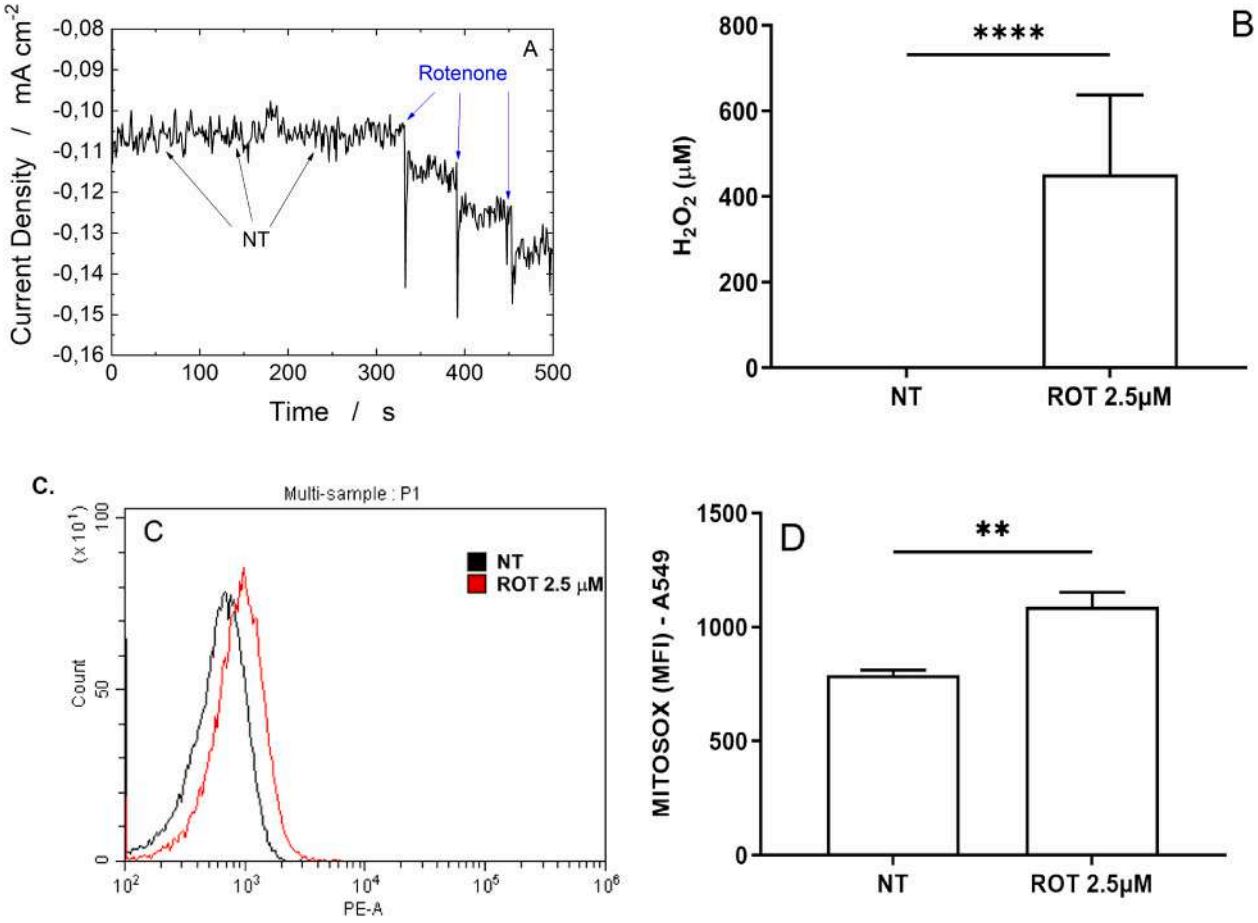

Fig. 10. A) Chronoamperogram for the hydrogen peroxide quantification in the conditioned medium used for non-treated (NT) and treated with 2.5 μM Rotenone (ROT)-treated A549 cells. B) Hydrogen peroxide concentration detected by the sensor. *p value < 0.05 Paired *t*-test (N = 3). C) Mitochondrial superoxide detection by flow cytometry using Mitosox Red probe: representative flow cytometric analysis. D) Mitochondrial superoxide production reported as Mean Fluorescence Intensity (MFI) ± SD (N = 3), *p < 0.05 Paired *t*-test.

average diameter of about 200 nm. The nanostructured shape of the electrode guarantees a high surface area about 7 times larger than that of a planar gold electrode. The H_2O_2 reduction process was studied by CV at various scan speeds and was found to be controlled by diffusion.

The AuNWs-based electrodes were tested for the detection of hydrogen peroxide by chronoamperometry applying a potential of −0.35 V vs SCE. The AuNW-based sensor had a limit of detection of 3.2 μM, a very wide linear range (from 10 μM to 10 mM) with a very high sensitivity of 0.98 μA $\mu M^{-1} cm^{-2}$. The sensor reproducibility and repeatability were very good because values of 3% and 7% were obtained. The sensor was also very stable. The selectivity of the sensor was good even in the presence of high concentrations of ascorbic acid, glucose, uric acid, nitrate ions, HEPES, lactic acid, sodium chloride and Rotenone.

The sensor was also validated by measuring the hydrogen peroxide released by human airway cells treated with Rotenone which induces mitochondrial damage and in turn oxidative stress. In particular, the conditioned medium of A549 cells treated and untreated with Rotenone was analyzed. The results were in according with those obtained by flow cytometry after staining the cells with a mithocondrial ROS-sensitive fluorescent probe. This highlights the great potential of the proposed electrochemical sensor as an innovative and alternative approach for the quantification of cellular oxidative stress.

CRediT authorship contribution statement

Bernardo Patella: Investigation, Methodology, Validation, Writing – original draft. **Serena Di Vincenzo:** Investigation, Methodology, Validation, Writing – original draft. **Nadia Moukri:** Data curation, Investigation, Resources. **Francesco Bonafede:** Data curation, Investigation, Resources. **Maria Ferraro:** Data curation, Formal analysis, Validation. **Valentina Lazzara:** Data curation, Formal analysis, Validation. **Maria Rita Giuffrè:** Data curation, Formal analysis, Validation. **Sonia Carbone:** Data curation, Investigation, Resources. **Giuseppe Aiello:** Funding acquisition, Project administration. **Michele Russo:** Funding acquisition, Project administration. **Chiara Cipollina:** Conceptualization, Supervision, Writing – review & editing. **Rosalinda Inguanta:** Conceptualization, Supervision, Writing – review & editing. **Elisabetta Pace:** Conceptualization, Supervision, Writing – review & editing.

Declaration of competing interest

The authors declare that they have no known competing financial interests or personal relationships that could have appeared to influence the work reported in this paper.

Data availability

No data was used for the research described in the article.

Acknowledgments

This research was supported by the University of Palermo, Italian National Research Council and Fondazione Ri.Med and has been financed by the Project “SeNSO” (n. 082651290364, linea di intervento 1.1.5 del P.35FESR Sicilia 2014/2020).

Appendix A. Supplementary data

Supplementary data to this article can be found online at https://doi.org/10.1016/j.talanta.2024.125772.

References

[1] H. Teymourian, M. Parrilla, J.R. Sempionatto, N.F. Montiel, A. Barfidokht, R. Van Echelpoel, K. De Wael, J. Wang, Wearable electrochemical sensors for the monitoring and screening of drugs, ACS Sens. 5 (2020) 2679–2700, https://doi.org/10.1021/acssensors.0c01318.
[2] B. O'Sullivan, S. O'Sullivan, T. Narayan, H. Shao, B. Patella, I. Seymour, R. Inguanta, A. O'Riordan, A direct comparison of 2D versus 3D diffusion analysis at nanowire electrodes: a finite element analysis and experimental study, Electrochim. Acta (2022) 139890, https://doi.org/10.1016/j.electacta.2022.139890.
[3] J.H. Kim, Y.J. Suh, D. Park, H. Yim, H. Kim, H.J. Kim, D.S. Yoon, K.S. Hwang, Technological advances in electrochemical biosensors for the detection of disease biomarkers, Biomed. Eng. Lett. 11 (2021) 309–334, https://doi.org/10.1007/s13534-021-00204-w.
[4] B. Patella, G. Aiello, G. Drago, C. Torino, A. Vilasi, A. O'Riordan, R. Inguanta, Electrochemical detection of chloride ions using Ag-based electrodes obtained from compact disc, Anal. Chim. Acta 1190 (2022) 339215, https://doi.org/10.1016/j.aca.2021.339215.
[5] R.K.A. Amali, H.N. Lim, I. Ibrahim, Z. Zainal, S.A.A. Ahmad, Silver nanoparticles-loaded copper (II)-terephthalate framework nanocomposite as a screen-printed carbon electrode modifier for amperometric nitrate detection, J. Electroanal. Chem. 918 (2022) 116440, https://doi.org/10.1016/j.jelechem.2022.116440.
[6] R.M. Silva, G.H. Sperandio, A.D. Da Silva, L.L. Okumura, R.C. Da Silva, R.P. L. Moreira, T.A. Silva, Electrochemically reduced graphene oxide films from Zn-C battery waste for the electrochemical determination of paracetamol and hydroquinone, Microchim. Acta 190 (2023) 273, https://doi.org/10.1007/s00604-023-05858-0.
[7] E. Fazio, S. Spadaro, C. Corsaro, G. Neri, S.G. Leonardi, F. Neri, N. Lavanya, C. Sekar, N. Donato, G. Neri, Metal-oxide based nanomaterials: synthesis, characterization and their applications in electrical and electrochemical sensors, Sensors 21 (2021) 2494, https://doi.org/10.3390/s21072494.
[8] S. Aralekallu, L.K. Sannegowda, Metal nanoparticles for electrochemical sensing applications, in: Handb. Nanomater. Sens. Appl., Elsevier, 2021, pp. 589–629, https://doi.org/10.1016/B978-0-12-820783-3.00001-4.
[9] B. O'Sullivan, B. Patella, R. Daly, I. Seymour, C. Robinson, P. Lovera, J. Rohan, R. Inguanta, A. O'Riordan, A simulation and experimental study of electrochemical pH control at gold interdigitated electrode arrays, Electrochim. Acta 395 (2021) 139113, https://doi.org/10.1016/j.electacta.2021.139113.
[10] M. Zhang, X. Guo, Gold/platinum bimetallic nanomaterials for immunoassay and immunosensing, Coord. Chem. Rev. 465 (2022) 214578, https://doi.org/10.1016/j.ccr.2022.214578.
[11] W.-J. Wang, M.-C. Chou, Y.-J. Lee, W.-L. Hsu, G.-J. Wang, A simple electrochemical immunosensor based on a gold nanoparticle monolayer electrode for neutrophil gelatinase-associated lipocalin detection, Talanta 246 (2022) 123530, https://doi.org/10.1016/j.talanta.2022.123530.
[12] M.H. Hussain, N.F. Abu Bakar, A.N. Mustapa, K.-F. Low, N.H. Othman, F. Adam, Synthesis of various size gold nanoparticles by chemical reduction method with different solvent polarity, Nanoscale Res. Lett. 15 (2020) 140, https://doi.org/10.1186/s11671-020-03370-5.
[13] I. Hammami, N.M. Alabdallah, A.A. jomaa, M. kamoun, Gold nanoparticles: synthesis properties and applications, J. King Saud Univ. Sci. 33 (2021) 101560, https://doi.org/10.1016/j.jksus.2021.101560.
[14] N. German, A. Ramanavicius, A. Ramanaviciene, Electrochemical deposition of gold nanoparticles on graphite rod for glucose biosensing, Sensor. Actuator. B Chem. 203 (2014) 25–34, https://doi.org/10.1016/j.snb.2014.06.021.
[15] E. Spain, A. McCooey, K. Joyce, T.E. Keyes, R.J. Forster, Gold nanowires and nanotubes for high sensitivity detection of pathogen DNA, Sensor. Actuator. B Chem. 215 (2015) 159–165, https://doi.org/10.1016/j.snb.2015.03.040.
[16] M. Wirtz, C.R. Martin, Template-fabricated gold nanowires and nanotubes, Adv. Mater. 15 (2003) 455–458, https://doi.org/10.1002/adma.200390106.
[17] B. Mohan Mundotiya, W. Ullah, Morphology controlled synthesis of the nanostructured gold by electrodeposition techniques, in: M. Sone, K. Masu (Eds.), Nov. Met. Electrodepos, Recent Appl., IntechOpen, 2019, https://doi.org/10.5772/intechopen.80846.
[18] T.-H. Lin, C.-W. Lin, H.-H. Liu, J.-T. Sheu, W.-H. Hung, Potential-controlled electrodeposition of gold dendrites in the presence of cysteine, Chem. Commun. 47 (2011) 2044, https://doi.org/10.1039/c0cc03273e.
[19] A. Sukeri, M. Bertotti, Electrodeposited honeycomb-like dendritic porous gold surface: an efficient platform for enzyme-free hydrogen peroxide sensor at low overpotential, J. Electroanal. Chem. 805 (2017) 18–23, https://doi.org/10.1016/j.jelechem.2017.10.004.
[20] J. Guiliani, J. Cadena, C. Monton, Template-assisted electrodeposition of Ni and Ni/Au nanowires on planar and curved substrates, Nanotechnology 29 (2018) 075301, https://doi.org/10.1088/1361-6528/aaa261.
[21] J. Zhang, J.H. Ma, J. Bai, D. Yang, M. Zhang, Z. Yang, L. Fan, X.L. Chen, R.G. Guan, A facile template-assisted electrodeposition approach to porous Cu/Cu_2O nanowires, RSC Adv. 11 (2021) 30215–30221, https://doi.org/10.1039/D1RA04770A.
[22] J.J. Boote, K. Critchley, S.D. Evans, Surfactant mediated assembly of gold nanowires on surfaces, J. Exp. Nanosci. 1 (2006) 125–142, https://doi.org/10.1080/17458080600669785.
[23] T. Tian, J. Dong, J. Xu, Direct electrodeposition of highly ordered gold nanotube arrays for use in non-enzymatic amperometric sensing of glucose, Microchim. Acta 183 (2016) 1925–1932, https://doi.org/10.1007/s00604-016-1835-2.

[24] S.R. Torati, V. Reddy, S.S. Yoon, C. Kim, Electrochemical biosensor for Mycobacterium tuberculosis DNA detection based on gold nanotubes array electrode platform, Biosens. Bioelectron. 78 (2016) 483–488, https://doi.org/10.1016/j.bios.2015.11.098.
[25] Y. Bahari Mollamahale, M. Ghorbani, A. Dolati, D. Hosseini, Electrodeposition of well-defined gold nanowires with uniform ends for developing 3D nanoelectrode ensembles with enhanced sensitivity, Mater. Chem. Phys. 213 (2018) 67–75, https://doi.org/10.1016/j.matchemphys.2018.04.004.
[26] Y. Bahari Mollamahalle, M. Ghorbani, A. Dolati, Electrodeposition of long gold nanotubes in polycarbonate templates as highly sensitive 3D nanoelectrode ensembles, Electrochim. Acta 75 (2012) 157–163, https://doi.org/10.1016/j.electacta.2012.04.119.
[27] M.K. Sharma, A.S. Ambolikar, S.K. Aggarwal, Electrochemical synthesis of gold nanorods in track-etched polycarbonate membrane using removable mercury cathode, J. Nanoparticle Res. 14 (2012) 1094, https://doi.org/10.1007/s11051-012-1094-z.
[28] C. Cipollina, A. Bruno, S. Fasola, M. Cristaldi, B. Patella, R. Inguanta, A. Vilasi, G. Aiello, S.L. Grutta, C. Torino, E. Pace, Cellular and molecular signatures of oxidative stress in bronchial epithelial cell models injured by cigarette smoke extract, Int. J. Mol. Sci. (2022) 22.
[29] M. Schieber, N.S. Chandel, ROS function in redox signaling and oxidative stress, Curr. Biol. 24 (2014) R453–R462, https://doi.org/10.1016/j.cub.2014.03.034.
[30] S.D. Vincenzo, G. Ferrante, M. Ferraro, C. Cascio, V. Malizia, A. Licari, S. La Grutta, E. Pace, Oxidative stress, environmental pollution, and lifestyle as determinants of asthma in children, Biology 12 (2023) 133, https://doi.org/10.3390/biology12010133.
[31] F.S. Bezerra, M. Lanzetti, R.T. Nesi, A.C. Nagato, C.P.E. Silva, E. Kennedy-Feitosa, A.C. Melo, I. Cattani-Cavalieri, L.C. Porto, S.S. Valenca, Oxidative stress and inflammation in acute and chronic lung injuries, Antioxidants 12 (2023) 548, https://doi.org/10.3390/antiox12030548.
[32] H. Shamkhalichenar, J.-W. Choi, Review—non-enzymatic hydrogen peroxide electrochemical sensors based on reduced graphene oxide, J. Electrochem. Soc. 167 (2020) 037531, https://doi.org/10.1149/1945-7111/ab644a.
[33] T. Ahmad, A. Iqbal, S.A. Halim, J. Uddin, A. Khan, S. El Deeb, A. Al-Harrasi, Recent advances in electrochemical sensing of hydrogen peroxide (H2O2) released from cancer cells, Nanomaterials 12 (2022) 1475, https://doi.org/10.3390/nano12091475.
[34] A. Sukeri, A.S. Lima, M. Bertotti, Development of non-enzymatic and highly selective hydrogen peroxide sensor based on nanoporous gold prepared by a simple unusual electrochemical approach, Microchem. J. 133 (2017) 149–154, https://doi.org/10.1016/j.microc.2017.03.023.
[35] L. Zhang, F. Chen, G. Ren, Z. Wang, Hydrogen peroxide electrochemical sensor based on gold nanoparticles modified with nitrogen-doped and nanoperforated graphene nanozymes, Funct. Mater. Lett. 15 (2022) 2250004, https://doi.org/10.1142/S1793604722500047.
[36] R. Zeis, T. Lei, K. Sieradzki, J. Snyder, J. Erlebacher, Catalytic reduction of oxygen and hydrogen peroxide by nanoporous gold, J. Catal. 253 (2008) 132–138, https://doi.org/10.1016/j.jcat.2007.10.017.
[37] K. Fu, J. Seo, V. Kesler, N. Maganzini, B.D. Wilson, M. Eisenstein, B. Murmann, H. T. Soh, Accelerated electron transfer in nanostructured electrodes improves the sensitivity of electrochemical biosensors, Adv. Sci. 8 (2021) 2102495, https://doi.org/10.1002/advs.202102495.
[38] B. Lafuente, R.T. Downs, H. Yang, N. Stone, 1. The power of databases: the RRUFF project, in: T. Armbruster, R.M. Danisi (Eds.), Highlights Mineral. Crystallogr., DE GRUYTER, 2015, pp. 1–30, https://doi.org/10.1515/9783110417104-003.
[39] M.B. Hariri, A. Dolati, R.S. Moakhar, The potentiostatic electrodeposition of gold nanowire/nanotube in $HAuCl_4$ solutions based on the model of recessed cylindrical ultramicroelectrode array, J. Electrochem. Soc. 160 (2013) D279–D288, https://doi.org/10.1149/2.141306jes.
[40] Z.-Y. Lv, A.-Q. Li, Y. Fei, Z. Li, J.-R. Chen, A.-J. Wang, J.-J. Feng, Facile and controlled electrochemical route to three-dimensional hierarchical dendritic gold nanostructures, Electrochim. Acta 109 (2013) 136–144, https://doi.org/10.1016/j.electacta.2013.07.123.
[41] J. Xiao, L. Qi, Surfactant-assisted, shape-controlled synthesis of gold nanocrystals, Nanoscale 3 (2011) 1383, https://doi.org/10.1039/c0nr00814a.
[42] X. Li, Y. Wang, G. Song, Z. Peng, Y. Yu, X. She, J. Li, Synthesis and growth mechanism of Ni nanotubes and nanowires, Nanoscale Res. Lett. 4 (2009) 1015, https://doi.org/10.1007/s11671-009-9348-0.
[43] Y. Fukunaka, M. Motoyama, Y. Konishi, R. Ishii, Producing shape-controlled metal nanowires and nanotubes by an electrochemical method, Electrochem. Solid State Lett. 9 (2006) C62, https://doi.org/10.1149/1.2165711.
[44] J.J. Díaz León, D.M. Fryauf, R.D. Cormia, N.P. Kobayashi, in: N.P. Kobayashi, A. A. Talin, M.S. Islam, A.V. Davydov (Eds.), Study of the Formation of Native Oxide on Copper at Room Temperature, San Diego, California, United States, 2016, p. 99240O, https://doi.org/10.1117/12.2238745.
[45] A.J. Bard, L.R. Faulkner, Electrochemical Methods: Fundamentals and Applications, second ed., Wiley, New York, 2001.
[46] V. Maciulis, A. Ramanaviciene, I. Plikusiene, Recent advances in synthesis and application of metal oxide nanostructures in chemical sensors and biosensors, Nanomaterials 12 (2022) 4413, https://doi.org/10.3390/nano12244413.
[47] F. Schröper, D. Brüggemann, Y. Mourzina, B. Wolfrum, A. Offenhäusser, D. Mayer, Analyzing the electroactive surface of gold nanopillars by electrochemical methods for electrode miniaturization, Electrochim. Acta 53 (2008) 6265–6272, https://doi.org/10.1016/j.electacta.2008.03.068.
[48] M. Gerlache, Züh Senturk, G. Quarin, J.-M. Kauffmann, Electrochemical behavior of H2O2 on gold, Electroanalysis 9 (1997) 1088–1092, https://doi.org/10.1002/elan.1140091411.
[49] Y. Zhang, Y. Sun, Z. Liu, F. Xu, K. Cui, Y. Shi, Z. Wen, Z. Li, Au nanocages for highly sensitive and selective detection of H2O2, J. Electroanal. Chem. 656 (2011) 23–28, https://doi.org/10.1016/j.jelechem.2011.01.037.
[50] H. Yin, S. Ai, W. Shi, L. Zhu, A novel hydrogen peroxide biosensor based on horseradish peroxidase immobilized on gold nanoparticles–silk fibroin modified glassy carbon electrode and direct electrochemistry of horseradish peroxidase, Sensor. Actuator. B Chem. 137 (2009) 747–753, https://doi.org/10.1016/j.snb.2008.12.046.
[51] X. Chen, Z. Cai, Z. Huang, M. Oyama, Y. Jiang, X. Chen, Ultrafine palladium nanoparticles grown on graphene nanosheets for enhanced electrochemical sensing of hydrogen peroxide, Electrochim. Acta 97 (2013) 398–403, https://doi.org/10.1016/j.electacta.2013.02.047.
[52] B. Patella, S.D. Vincenzo, C. Zanca, L. Bollaci, M. Ferraro, M.R. Giuffrè, C. Cipollina, M.G. Bruno, G. Aiello, M. Russo, R. Inguanta, E. Pace, Electrochemical quantification of H2O2 released by airway cells growing in different culture media, Micromachines 13 (2022) 1762, https://doi.org/10.3390/mi13101762.
[53] S. Di Vincenzo, C. Sangiorgi, M. Ferraro, M. Buscetta, C. Cipollina, E. Pace, Cigarette smoke extract reduces FOXO3a promoting tumor progression and cell migration in lung cancer, Toxicology 454 (2021) 152751, https://doi.org/10.1016/j.tox.2021.152751.
[54] I. Sipos, L. Tretter, V. Adam-Vizi, The production of reactive oxygen species in intact isolated nerve terminals is independent of the mitochondrial membrane potential, Neurochem. Res. 28 (2003) 1575–1581, https://doi.org/10.1023/A:1025634728227.